INSTITUT DE FRANCE
Académie des sciences

Comptes Rendus

Chimie

Ammar Mlayah, Salah Jellali, Ahmed Amine Azzaz, Mejdi Jeguirim, Haykel Sellalmi and Noureddine Hamdi

Investigations on lignite use for lead removal from aqueous solutions under static and dynamic conditions: adsorption properties and mechanism exploration

Volume 24, Special Issue S1 (2021), p. 7-22

Published online: 4 March 2021
Issue date: 4 November 2021

https://doi.org/10.5802/crchim.71

Part of Special Issue: Sustainable Biomass Resources for Environmental, Agronomic, Biomaterials and Energy Applications 2

Guest editors: Mejdi Jeguirim (Institut de Science des Matériaux de Mulhouse, France), Salah Jellali (Sultan Qaboos University, Oman) and Besma Khiari (Water Research and Technologies Centre, Tunisia)

Les Comptes Rendus. Chimie *sont membres du*
Centre Mersenne pour l'édition scientifique ouverte
www.centre-mersenne.org
e-ISSN : 1878-1543

Comptes Rendus
Chimie
2021, 24, nº S1, p. 7-22
https://doi.org/10.5802/crchim.71

Sustainable Biomass Resources for Environmental, Agronomic, Biomaterials and Energy Applications 2 / *Ressources de biomasse durables pour des applications environnementales, agronomiques, de biomatériaux et énergétiques 2*

Investigations on lignite use for lead removal from aqueous solutions under static and dynamic conditions: adsorption properties and mechanism exploration

Ammar Mlayah [a], Salah Jellali [*, b], Ahmed Amine Azzaz [c], Mejdi Jeguirim [c], Haykel Sellalmi [a] and Noureddine Hamdi [d]

[a] Georesources Laboratory, Water Research and Technologies Center (CERTE), Echo park of Borj Cedria, Carthage University, BP 273, Soliman 8020, Tunisia

[b] PEIE Research Chair for the Development of Industrial Estates and Free Zones, Centre for Environmental Studies and Research (CESAR), Sultan Qaboos University, Al-Khoud 123, Sultanate of Oman

[c] Université de Strasbourg, Université de Haute-Alsace, CNRS, Institut de Science des Matériaux de Mulhouse (IS2M) UMR 7361, F-68100 Mulhouse, France

[d] Higher Institute of Water Sciences and Techniques of Gabes, 6072 Zrig, Gabes, Tunisia

E-mails: ammarmlayah17@gmail.com (A. Mlayah), s.jellali@squ.edu.om (S. Jellali), amine.azzaz@uha.fr (A. A. Azzaz), mejdi.jeguirim@uha.fr (M. Jeguirim), haysellami@yahoo.fr (H. Sellalmi), nouryhamdi@gmail.com (N. Hamdi)

Abstract. Lignite, as an abundant and low-cost material, was tested for lead (Pb(II)) removal from aqueous solutions under various experimental conditions for both static (batch) and dynamic (column) experiments. Static assays showed that Pb(II) removal efficiency increases with rising in its initial concentration, aqueous pH, and adsorbent dosage values. Adsorption kinetic and isothermal data were well fitted with the pseudo-second-order and Freundlich models, respectively, suggesting that lead removal by lignite is mainly governed by chemical processes and occurs heterogeneously on multilayer surfaces. The maximum Langmuir's adsorption capacity was equal to 61.4 $mg{\cdot}g^{-1}$, which is high in comparison to various natural materials. The laboratory column experiments showed that Pb(II) breakthrough curves and subsequent lignite adsorption efficiency is highly dependent on the bed height. Due to the short time contact between Pb(II) and lignite particles inside the column, the highest adsorption capacity was about 21%, which is lower than the one found in the batch mode. Even under dynamic conditions, lignite exhibits a high adsorption capacity compared to other adsorbents, which promotes its use as a low-cost and efficient material for Pb(II) and the removal of other heavy metals from wastewaters.

[*] Corresponding author.

Keywords. Lignite, Lead removal, Batch, Column, Adsorption mechanisms.
Available online 4th March 2021

1. Introduction

Heavy metals are discharged in wastewaters from various industries including mining, batteries, fertilizers, and electronic and chemical processes. Even at low concentrations, some of these metals could be serious threats to the environment and human health [1]. Lead component (Pb(II)) has been pointed out as one of the most toxic heavy metals [2]. Indeed, this substance is not easily biodegradable and has a great bioaccumulation in some components of the food chain, which could seriously damage the human nervous, reproductive, and circulatory systems [2].

Thus, it is not surprising that during the last two decades, many research approaches and procedures have been developed to assess the removal of heavy metals, in particular Pb(II), from wastewaters [3] using a broad range of technologies including chemical precipitation, reduction, and membrane separation [3]. While these techniques can exhibit good removal performances under some specific conditions, they are often criticized since they are relatively costly and not eco-friendly, which has hindered their wide applications for real cases. For that reason, retention of heavy metals by both raw and modified materials has emerged as a practical alternative with simple design and easy operation, and an economically viable technique [4]. This method also has the main assets of reducing the use of chemicals, the reuse of the regenerated adsorbents, and the recovery of metals in line with the circular economy and sustainable development concepts [5,6]. Various organic and mineral supports have been tested for Pb(II) removal from both real wastewaters and synthetic solutions. They include several raw and modified agricultural and industrial biomasses [7,8] as well as mineral materials such as clays and marble wastes [9,10].

Lignite is a natural brown coal deposit that exists in many countries such as Indonesia, Australia, China, Russia, United States of America, and several European Union countries. According to recent statistics of the International Energy Agency, more than 2/3 of the global coal exports are insured by Indonesia, Australia, and Russia [11]. Nowadays, lignite is mainly used for electricity and gas generation as well as fertilizer production [11]. In the environmental sector, lignite has been tested as raw or modified material for the removal of various pollutants from aqueous solutions such as nutrients [12], dyes [13], pharmaceuticals [14], and heavy metals [15]. However, the majority of these studies were performed in small-volume flasks (static conditions). The extrapolation of the obtained batch results to real cases is often very difficult to perform due to the complexity of the real wastewater composition and its important variation in time along with its flow rate [8,16]. Therefore, studying Pb(II) removal in continuous mode (i.e., laboratory columns or continuous stirring tank reactor) is closer to the reality and will have an important added value compared to the static assays. This kind of assays is very helpful for the design, conception of large-scale adsorption devices, and also for the simulation of pollutant transfer and transport in the underground compartments through tailored numerical models [8]. Indeed, various parameters, determined at this laboratory scale such as kinetic adsorption rates, maximal adsorption capacities, isotherms coefficients, and minimal necessary contact time, are required as model inputs for upscaling purposes.

The main objectives of this study were: (i) to investigate the Pb(II) removal efficiencies by a Tunisian local lignite under various experimental conditions in both batch and column modes, (ii) to compare the found lignite's adsorption capacity ($mg{\cdot}g^{-1}$) with other materials reported in the bibliography, and (iii) to explore the involved adsorption mechanisms through kinetic, isothermal modeling, and various sophisticated analytical equipment.

2. Materials and methods

2.1. *Adsorbent preparation and characterization*

The used adsorbent in this research was collected from the Cap Bon deposit (north east of Tunisia). Prior to the adsorption tests, the lignite was dried overnight at 60 °C, and then sieved with an electric sieve shaker for 20 min. The fraction with diameter

size lower than 63 μm was used for the adsorption tests. The physico-chemical characterization of the lignite has concerned its mineral composition assessment by using an X-ray fluorescence spectrophotometer (Philips, Eindhoven, Netherlands), the determination of its BET specific surface area through N_2 gas adsorption method by using a gas adsorption analyzer, Quantachrome Autosorb 1 sorptometer. Furthermore, in order to predict the dominating surface charge of the lignite, the pH of zero-point-charge (pH_{ZPC}) value was assessed using the method described in the literature [17,18]. During these assays, 0.2 g of lignite was stirred for 24 hours in an NaCl solution (0.1 M) with initial pH values varying between 2 and 12 (Model 710 pH meter, Metrohm, Switzerland). The pH_{ZPC} value corresponds to the intersection point with the horizontal axis of the plot giving $\Delta pH = pH_{initial} - pH_{final}$ versus $pH_{initial}$.

Additional analyses of the lignite material before and after Pb(II) adsorption were performed for an accurate assessment of the involved mechanisms. These include the use of: (i) scanning electron microscopy (SEM) coupled with energy dispersive X-ray (EDX) (Philips model FEI model Quanta 400 apparatus, Amsterdam, The Netherlands) for microscopic images and qualitative composition of the materials, respectively; (ii) a TGA/DSC3+ apparatus (Mettler Toledo, Greifensee, Switzerland) for proximate analysis; (iii) a powder X-ray diffraction (XRD) by using a Panalytical X'Pert powder diffractometer (Malvern, UK) equipped with a copper anode for the identification of the present crystalline phases through the ICDD database of the Panalytical High score software; and (iv) a Fourier transform infrared (FTIR) analysis using a Magna-IR 560 NICOLET spectrometer. The FTIR spectra of the material before and after Pb(II) adsorption was assessed between 4000 and 400 cm^{-1} for a resolution of 1 cm^{-1}.

2.2. *Lead solutions preparation and analysis*

A lead aqueous solution at a concentration of 1 $g{\cdot}L^{-1}$ was prepared by using lead nitrates ($Pb(NO_3)_2$), acquired from Fisher Scientific, and distilled water. This solution was used during this study for the preparation of adsorption solutions at given Pb(II) concentrations. Lead concentrations, either in batch or column experiments, were measured using an atomic absorption spectrometer with an air–acetylene flame (Perkin Elmer AAnalyst200). The initial pH values of the solutions were adjusted by using dilute solutions (0.1 M) of nitric acid or sodium hydroxide.

2.3. *Static adsorption experiments*

Static (batch) investigations were carried out in order to determine the impact of the lignite granulometry including the contact time and initial Pb(II) concentrations, the initial aqueous pH values, the adsorbent dosages, and the presence of other competitive ions on Pb(II) removal efficiencies by lignite. All these assays were performed at a room temperature of 20 ± 2 °C in 120 mL capped flasks by shaking a given mass of lignite with 50 mL of aqueous solution at 400 rpm by using a Variomag-poly15 magnetic stirrer. Then, the suspension was filtered by a paper filter before analysis with the atomic absorption apparatus. During these assays, the default following factors were used: a lignite fraction with size lower than 63 μm, an initial Pb(II) concentration of 100 $mg{\cdot}L^{-1}$, an initial pH equal to 5, and a lignite dosage of 2 $g{\cdot}L^{-1}$.

The impact of the grain size effect was studied for the following lignite size fractions: lower than 63 μm, between 63 and 500 μm, 500–1000 μm, and 1000–2000 μm. The effect of contact time was determined for times of 0.17, 0.25, 0.5, 1, 5, 10, 20, 40, 60, and 90 min for initial Pb(II) concentrations of 15, 30, 50, 80, 100, 125, 150, and 175 $mg{\cdot}L^{-1}$. The impact of the aqueous pH was assessed for initial values of 2.0, 3.0, 4.0, and 5.0. The lignite dosage impact was deduced from separated assays using doses of 0.4, 1.0, 1.6, 2.0, 2.4, 3, 3.5, and 4.0 $g{\cdot}L^{-1}$. Finally, the competing effect with Pb(II) was determined in the presence of Cd(II), Cu(II), and Zn(II) in a mixed solution. All of these metals exist at initial concentrations of 30 $mg{\cdot}L^{-1}$.

At a given moment "t," the adsorbed Pb(II) amount (q_t) and the related removal yield (Y_t) were determined as follows:

$$q_t = \frac{(C_0 - C_t)}{D} \tag{1}$$

$$Y_t(\%) = \frac{(C_0 - C_t)}{C_0} \times 100, \tag{2}$$

where C_0 and C_t are the initial and at time "t" Pb(II) concentrations, respectively ($mg{\cdot}L^{-1}$). D is the adsorbent dosage ($g{\cdot}L^{-1}$).

In this work, the kinetic Pb(II) adsorption data were fitted to the well-known models: pseudo-first-order (PFO), pseudo-second-order (PSO), and

intraparticle and film diffusion models. Moreover, at equilibrium, the experimental isothermal data (adsorbed amounts versus residual aqueous concentrations) were confronted to Freundlich, Langmuir, and Dubinin–Radushkevich (D–R) models. The original as well as the linearized equations of these kinetic and isothermal models were widely cited in the bibliography [10,19–21]. The agreement between the experimental and calculated adsorbed amounts by the kinetic and isothermal models was determined through the calculus of both the average percentage errors (APE) and the Akaike information criterion (AIC) [22,23].

$$\mathrm{APE}(\%) = \frac{\sum |(q_{\mathrm{exp}} - q_{\mathrm{theo}})/q_{\mathrm{exp}}|}{N} \times 100 \qquad (3)$$

$$\mathrm{AIC} = NLn\left(\frac{\mathrm{SSE}}{N}\right) + 2N_p + \frac{2N_p(N_p+1)}{N-N_p-1} \qquad (4)$$

$$\mathrm{SSE} = \sum_{i=1}^{i=N} (q_{\mathrm{exp}} - q_{\mathrm{theo}})^2, \qquad (5)$$

where q_{exp} and q_{theo} (mg/g) are the experimental and theoretical adsorbed amounts assessed by the used models, respectively. N is the number of experimental points in the kinetic/isotherm, N_p is the number of fitted parameters, and SSE is the residual sum of squares.

These two parameters (APE and AIC) are essential for the selection of the best fitting model to the experimental data. The model presenting the lowest values of these two parameters fits the best to the experimental data [22,23]. It is important to underline that in this work, we omitted the use of the determination coefficients (R^2) because they are not always suitable for the evaluation of the goodness of the fitting of equations to experimental data [23]. This is justified by the fact that the R^2 values calculus does not consider the degree of freedom of the used models equations [23].

2.4. *Dynamic adsorption experiments*

The experimental setup used for the study of Pb(II) removal efficiency in continuous mode consists of a plexiglass column having a total length and an internal diameter of 20 and 2.9 cm, respectively (Figure 1).

The preparation of these assays consisted of the lignite packing inside the column with small increments in order to avoid any preferential flow which would significantly affect the quality and precision of

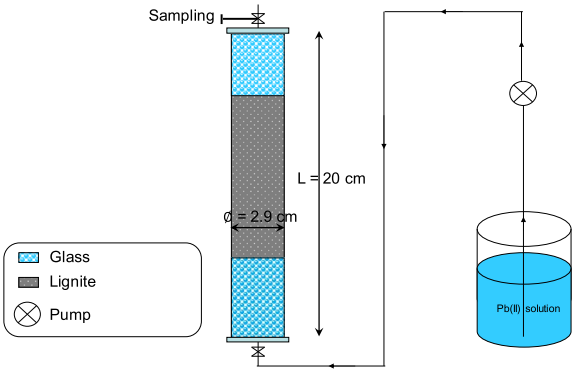

Figure 1. Schematic representation of the used column for studying Pb(II) removal by lignite under dynamic conditions.

Pb(II) breakthrough curves. In order to have a uniform flow through the porous media, glass particles were put in the two boundaries of the column [24]. The Pb(II) adsorption experiments consisted of the determination of the impact of the lignite bed height on Pb(II) removal efficiency for a constant flow rate, Pb(II) concentration, and aqueous pH of the feeding solution of 60 mL·min^{-1}, 100 mg·L^{-1}, and 5.0, respectively. Three bed heights were tested: 1.0, 1.5, and 2.0 cm. They correspond to lignite masses of 5, 7.5, and 10 g, respectively. The synthetic Pb(II) solution was pumped into the column in upward flow by using an adapted peristaltic pump (Masterflex®, USA). The time progress of the Pb(II) concentrations at the exit of the column was assessed through the analysis of aqueous solutions sampled at various times. When the measured Pb(II) concentration at the outlet of the columns became equal to the feeding solution, it is assumed that all adsorption sites were saturated and experiments were therefore stopped. In parallel to the Pb(II) adsorption studies, column conservative tracer experiments (no reaction with lignite) were performed under the same hydraulic conditions by using calcium chloride synthetic solutions (5 g·L^{-1}). Similar to the Pb(II) adsorption experiments, when the measured Cl^- concentrations at the exit of the column (by a calibrated specific electrode (Windaus LF538)) become equal to the pumped solution, experiments were stopped.

The experimental adsorbed Pb(II) masses (M_{ads}) per gram of lignite (q_{sat}) during the column assays

were determined through the trapezoidal rule approximation [16]:

$$q_{sat} = M_{ads}/M = C_{0,Pb(II)}\left[\int_0^{V_{tot}} \frac{C_{tr}}{C_{0,tr}}\,dv - \int_0^{V_{tot}} \frac{C_{Pb(II)}}{C_{0,Pb(II)}}\,dv\right]\Big/ M$$
$$= \left((C_{0,Pb(II)}/2)\left[\sum_{i=0}^{i=n}\left(\frac{C_{tr,i}+C_{tr,i+1}}{C_{0,tr}}\right)(V_{i+1}-V_i) - \sum_{j=0}^{j=n}\left(\frac{C_{Pb(II),j}+C_{Pb(II),j+1}}{C_{0,Pb(II)}}\right)(V_{j+1}-V_j)\right]\right)\Big/ M, \quad (6)$$

where $C_{0,Pb(II)}$ and $C_{0,tr}$ are the initial Pb(II) and the conservative tracer concentrations, respectively; $C_{Pb(II)}$ and C_{tr} are the measured Pb(II) and tracer concentrations at the exit of the column, V_{tot} is the water volume collected at the outlet of the column at the end of the experiment, $C_{tr,i}$; $C_{tr,i+1}$ are the tracer measured concentrations at the times "i" and "$i+1$," respectively; and $C_{Pb(II),j}$, $C_{Pb(II),j+1}$ are the Pb(II) measured concentrations at moments "j" and "$j+1$," respectively. Finally, M is the mass of lignite.

3. Results and discussion

3.1. *Preliminary characterization of the adsorbent*

This section presents some preliminary but important properties of the raw lignite fraction with particle size lower than 63 μm. Other characteristics will be presented later in Section 3.3 when exploring the probable adsorption mechanisms of Pb(II) onto lignite particles.

The mineral composition of the raw lignite is summarized in Table 1 with the total contents of Na, K, Ca and Mg, which were low (about 1.9%). The highest contents were registered for silica (6.2%), sulfur (5.1%), iron (2.6%), and aluminum (2.5%). Some of these elements could be exchanged with Pb(II) during its adsorption by lignite.

The BET surface area of the lignite was assessed to 11.2 $m^2 \cdot g^{-1}$. It is relatively important compared to the values found for lignite from Serbia [25] and Greece [26] who reported values of 1.0 and 3.6 $m^2 \cdot g^{-1}$, respectively. It is also higher than waste fungal biomass [27] and other classic raw agricultural biomasses such as peanut shell [28]. It indicates that the lignite could exhibit high Pb(II) adsorption capacities. On the other hand, the pH_{ZPC} of the lignite was estimated to 3.6, which is quite similar to the value found by Mohan and Chander [29] for an American lignite. The relatively low found pH_{ZPC} indicates that this adsorbent could effectively remove Pb(II) for a wide pH range through electrostatic reactions. Indeed, for pH values higher than the pH_{ZPC}, the lignite particles' surface will be mainly negatively charged and consequently the Pb(II) retention will be favored [8].

Table 1. Mineral elemental analysis of the raw lignite

Element	Content (%, dry basis)
Na	0.06
K	0.46
Ca	1.21
Mg	0.21
Al	2.48
Fe	2.6
P	0.04
Cl	0.21
Si	6.15
S	5.12

3.2. *Static adsorption results*

3.2.1. *Effect of the size distribution of lignite particles*

The impact of size distribution of lignite particles on Pb(II) removal was performed under the experimental conditions presented in Section 2.3. Results (Figure 2) demonstrated that the finer the lignite fraction, the more important the Pb(II) removal efficiency. In fact, the most important adsorbed amount (43.2 $mg \cdot g^{-1}$) was registered for the lignite having the finest fraction (<63 μm). This quantity decreases with the increase of the particle size and reaches only 15.8 $mg \cdot g^{-1}$ for lignite particle dimension between 1 and 2 mm. This finding could be imputed to the more developed texture characteristics for lower lignite particle size dimensions, especially specific surface area (SSA) and microporosity [30,31]. Gunawardana *et al.* [30] assessed the variation on SSA versus particle size of a local soil (Dermosol and Kurosols in

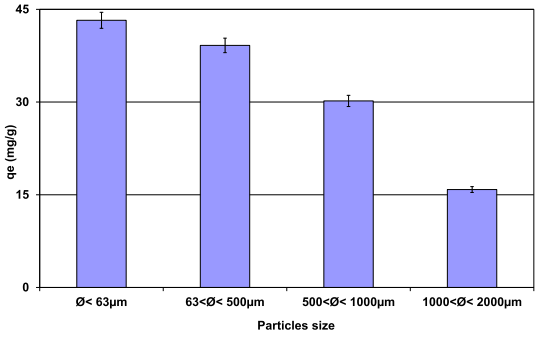

Figure 2. Impact of lignite particle size distribution on the Pb(II) removal by lignite (D = 2 g·L^{-1}; t = 90 min; C_0 = 100 mg·L^{-1}; pH$_0$ = 5; T = 20 ± 2 °C).

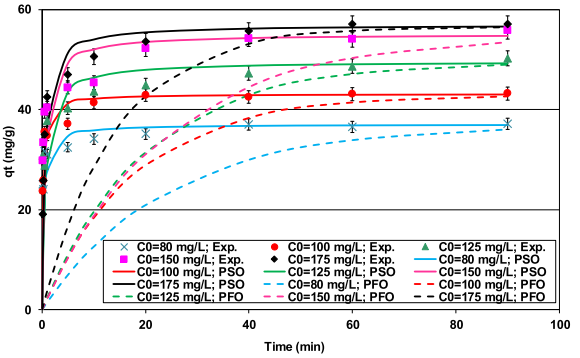

Figure 3. Impact of the contact time and initial aqueous concentrations on the Pb(II) removal by lignite (D = 2 g·L^{-1}; pH$_0$ = 5; T = 20 ± 2 °C).

Australia). They showed that the SSA of particles with size lower than 75 µm is about four times larger than the one reported for the same soil with particle size ranging from 300 to 425 µm. This ratio reaches more than 17 for atmospheric aerosols for average particle size diameters of 0.6 and 8.8 µm [31]. Similar behavior was observed by PN and CP [32] and Kumar *et al.* [33] when investigating an oily effluent treatment by hard wood-based adsorbents and phosphorus by various porous metal oxides. For instance, PN and CP [32] reported that for a contact time of 4 hours, an increase of the average size particles from 0.8 mm to 3.5 mm resulted in a decrease of the removal efficiency by about 30%.

3.2.2. *Effect of contact time and initial concentrations—kinetic study*

The lignite seems to be an effective material for the removal of Pb(II) from the synthetic effluents since for initial concentrations of 15, 30, and 50 mg·L^{-1}, lead ions were completely removed (data not shown). For initial concentrations higher than 80 mg·L^{-1}, it appears that Pb(II) removal efficiency by the lignite is obviously a time- and concentration-dependent process (Figure 3). In fact, Pb(II) removal is exceptionally rapid till 0.5 min with an adsorption amount of 83% of the removed one at equilibrium starting at an initial concentration of 100 mg·L^{-1} (Figure 3). This finding suggests that Pb(II) elimination occurs mainly through external surface reactions. The high reactivity of lignite represents an important asset when scaling up such process since it would permit an important energy saving. After the contact duration, the Pb(II) ions entered into the lignite particles and were internally adsorbed with slower rates. Equilibrium, corresponding to almost constant adsorbed amounts, was reached for a contact time of 20 min for lower initial concentrations and for 40 to 60 min for much higher Pb(II) aqueous concentrations (Figure 3). This plateau corresponds to the saturation of adsorption sites of the lignite. This trend is in concordance with those reported by Dong *et al.* [34] and Pentari *et al.* [26] when studying Pb(II) removal by a lignite-based activated carbon and a raw Greek lignite, respectively.

It is worth mentioning that at equilibrium the Pb(II) removal efficiency was significantly improved when increasing the initial Pb(II) concentration. For instance, the Pb(II) removed amount for an initial concentration of 80 mg·L^{-1} (36.9 mg·g^{-1}) has increased by more than 53%, when the Pb(II) concentration rose up to 175 mg·L^{-1}. This could be related to the presence of higher concentration gradients that provides important forces and diffusion rates permitting to tackle the Pb(II) mass transfer resistances between the aqueous and lignite particles [35–37]. Furthermore, for higher initial aqueous concentrations, the contact probability between lead ions and the lignite particles is more privileged [38].

The parameters of the three used kinetic models: PFO, PSO, and film and intraparticle diffusion models are given in Table 2.

It can be clearly seen from Table 2 and Figure 3 that the PSO model displays better fitting to the experimental data compared to the PFO model. Indeed,

Table 2. Kinetic parameters of Pb(II) removal by lignite ($D = 2$ g·L^{-1}; pH$_0 = 5$; $T = 20 \pm 2$ °C)

	Initial Pb(II) aqueous concentration (mg·L^{-1})				
	80	100	125	150	175
Exp. $q_{e,\text{exp}}$ (mg·g^{-1})	36.9	42.9	49.5	54.7	56.6
PFO model					
k_1 (min^{-1})	0.042	0.056	0.050	0.042	0.070
APE (%)	60.2	56.1	55.9	59.4	51.4
AIC	66.5	67.6	68.7	71.7	68.0
PSO model					
$q_{e,\text{theo}}$ (mg·g^{-1})	37.0	43.1	49.6	55.1	56.9
K$_2$ (g·mg^{-1}·min^{-1})	0.080	0.100	0.029	0.031	0.032
APE (%)	14.3	6.9	20.3	19.0	11.6
AIC	41.1	28.6	51.0	50.8	36.6
Film and intraparticle diffusion model					
D_f ($\times 10^{-14}$·m^2·s^{-1})	26.1	50.0	17.8	20.0	21.4
D_{ip} ($\times 10^{-14}$·m^2·s^{-1})	2.7	10.9	2.1	3.8	3.5

for all the studied concentrations, the calculated PSO model's APE and AIC were much lower than the ones corresponding to the PFO. Besides, the estimated PSO model's Pb(II) theoretical adsorbed amounts at equilibrium ($q_{e,\text{theo}}$) were in good agreement with the experimental ones (Table 2 and Figure 3) with a maximum difference percentage of 0.73% (observed for $C_0 = 150$ mg·L^{-1}). Consequently, the PSO model is more appropriated for fitting the Pb(II) retention by the lignite under the studied experimental conditions. This model suggests that the rate limiting step might be mainly a chemical process. It would essentially involve a cationic exchange mechanism between Pb(II) in the aqueous solution and monovalent/divalent cations on the lignite's surface [3]. The adsorption of Pb(II) by the lignite was also analyzed through the application of the film and intraparticle diffusion models. The results (Table 2) indicated that Pb(II) adsorption process proceeds mainly by surface interactions for times shorter than 1 min and by intraparticle diffusion at later stages (Figure 3). The calculated film diffusion coefficients were much higher than those related to intraparticle transfer process, confirming the low development of porosity and the specific surface area of the lignite. The corresponding ratios varied between 4.6 and 9.8 for initial Pb(II) concentrations of 100 and 80 mg·L^{-1}, respectively.

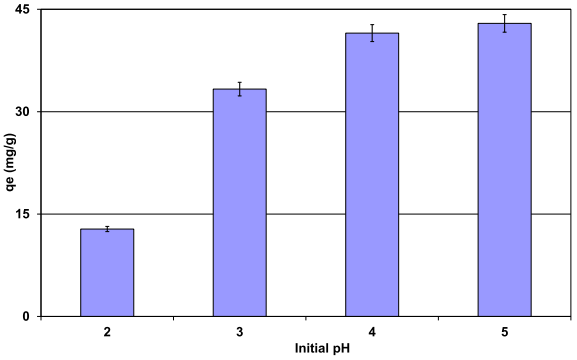

Figure 4. Impact of the initial aqueous pH on Pb(II) removal efficiency by lignite ($D = 2$ g·L^{-1}; $t = 90$ min; $C_0 = 100$ mg·L^{-1}; $T = 20 \pm 2$ °C).

These results suggest that the intraparticle diffusion process could be the limiting factor during Pb(II) adsorption by the lignite (Table 2). Similar findings were reported by Tsibranska and Hristova [39] when studying the adsorption of heavy metals by an activated carbon derived from apricot stones.

3.2.3. *Effect of initial aqueous pH*

The impact of the initial aqueous pH on Pb(II) removal efficiency by the lignite was performed under the experimental conditions given in Section 2.3. The

experimental results (Figure 4) showed that the removed Pb(II) amounts increased with the increase of the aqueous pH. Indeed, for an initial pH of 2, the Pb(II) adsorbed amount was only about 12.8 mg·g^{-1}. It increases by about 235% for an initial pH of 5, reaching a value of 42.9 mg·g^{-1}. This finding is mainly imputed to the surface charges of lignite particles. Indeed, for aqueous pH lower than the pH_{ZPC} (3.6), the lignite particle surfaces are positively charged, which repulses the cationic metal Pb(II). Furthermore, at this pH range, H^+ ions will compete with Pb(II) to be fixed on the available adsorption sites [40]. However, when the pH values are higher than the pH_{ZPC}, the adsorbent surfaces will carry more negative charges and, thus, prevailing the Pb(II) retention through electrostatic reactions. This trend was also reported by several studies dealing with the removal of heavy metals by raw and modified materials [41–43]. It is worth mentioning that precipitation of Pb(II) as $Pb(OH)_2$ (lead oxide), $PbCO_3$ (cerussite), and $Pb_3(CO_3)_2(OH)_2$ (hydrocerussite) has been reported as an important removal mechanism for mixed aqueous solutions with relatively high alkaline pH values [42]. In our case, this mechanism should be absent because of the low pH values of both lignite and tested aqueous range.

3.2.4. *Effect of lignite dosage*

The experimental results indicated that for lignite dosages lower than 3 g·L^{-1}, the Pb(II) removal efficiency highly increases with the increase of the adsorbent dosage (Figure 5). Indeed, for an initial Pb(II) initial concentration of 100 mg·L^{-1}, the measured removal yields increased from 36.2% to more than 90.7% when the lignite dose rose from 0.4 g to 3 g·L^{-1} (Figure 5).

This significant increase could be imputed to the presence of more available adsorption sites on the surface of the lignite particles. For doses higher than 3 g·L^{-1}, Pb(II) removal yields remained quasi-constant with average removal yields and residual aqueous concentrations of 92.3% and 7.7 mg·L^{-1}, respectively. Similar trends were reported by Jain *et al.* [44] and Dong *et al.* [34] when investigating metal removal from aqueous solutions by copper oxide nanoparticles and a lignite-derived-activated carbon, respectively. Thus, under the studied experimental conditions, lignite can be considered as a promising and attractive material for Pb(II) removal from industrial effluents since only relatively low dosages are able to perform high removal yields.

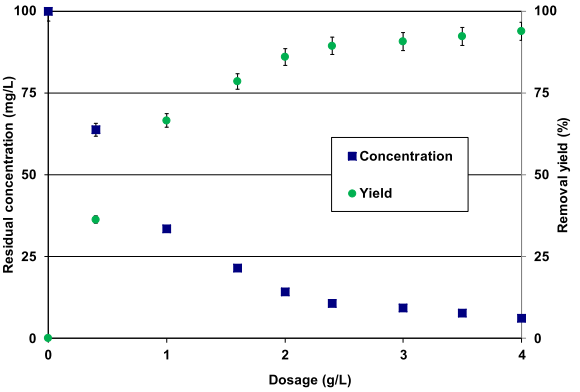

Figure 5. Impact of the lignite dosage on Pb(II) removal (t = 90 min; C_0 = 100 mg·L^{-1}; pH_0 = 5; $T = 20 \pm 2$ °C).

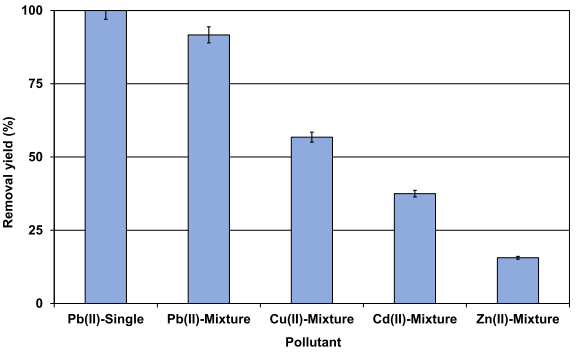

Figure 6. Impact of the presence of other metals on Pb(II) removal efficiency (D = 2 g·L^{-1}; t = 90 min; C_0 = 100 mg·L^{-1}; pH_0 = 5; $T = 20 \pm 2$ °C).

3.2.5. *Competing effect*

Since the industrial effluents always contain a mixture of dissolved heavy metals, the lignite sorption selectivity was also assessed in presence of Pb(II), Cu(II), Cd(II), and Zn(II) at initial concentration of 30 mg·L^{-1} for each of them (Section 2.3). Results (Figure 6) indicated that in the presence of the three other metals, Pb(II) removal yield has decreased from 100% to 91.7%.

This finding is imputed to the Pb(II) competition with the other metals for the same adsorption sites. It is however important to underline

Table 3. Adsorption isotherm parameters of Pb(II) removal by lignite (D = 2 g·L^{-1}; t_0 = 90 min; C_0 = 100 mg·L^{-1}; pH$_0$ = 5; T = 20 ± 2 °C)

Freundlich model	
Freundlich constant: K_F	25.8
Freundlich constant: n	5.1
APE (%)	1.5
AIC	9.2
Langmuir model	
Langmuir's maximum adsorption capacity; q_m (mg·g^{-1})	61.4
Langmuir constant: K_L	0.191
APE (%)	3.5
AIC	16.5
D–R model	
$q_{m,\text{D–R}}$ (mg·g^{-1})	115.5
E (kJ·mol^{-1})	16.7
APE (%)	1.1
AIC	7.7

that the order of retention preference is as follows: Pb(II)>Cu(II)>Cd(II) and Zn(II) with removal yields of 91.7%, 56.8%, 37.5%, and 15.6%, respectively (Figure 6). Therefore, in case of real wastewaters containing various heavy metals, P(II) and Cu(II) will be preferentially retained compared to the other metals. Various reasons were cited as an explanation for this behavior. They mainly include the metal size, electronegativity, availability, and hydration energy [7,42]. Similar trends have been observed by

Doskocil and Pekar [38] and Binabaj and Ramezanian [45] when studying the removal of metal ions from a multicomponent mixture using a natural lignite and nature-derived adsorbents (brown coal and zeolite).

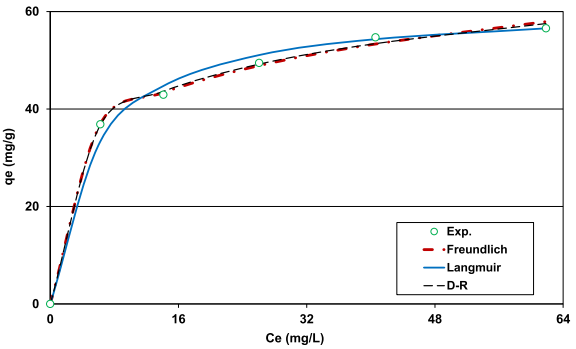

Figure 7. Fitting of the Pb(II) adsorption onto lignite experimental data to Freundlich, Langmuir, and D–R models (D = 2 g·L^{-1}; t_0 = 90 min; C_0 = 100 mg·L^{-1}; pH$_0$ = 5; T = 20 ± 2 °C).

3.2.6. *Isotherm adsorption*

The results of the experimental data fitting to Freundlich, Langmuir, and D–R models are given by Figure 7 and Table 3. It can be seen on Figure 7 that the three models fitted well to the measured data. However, even if the calculated APE and AIC for the D–R model were the lowest, the corresponding Pb(II) adsorption capacity was much higher than the expected one (115.5 mg·g^{-1}, Table 3) and seems to be unrealistic given the experimental isotherm shape (Figure 6). This finding could be imputed to this model's assumptions, especially the one related to the uniformity and homogeneity of the studied adsorbent microporous structure [20]. It is important to underline that the calculated free energy ($E = 1/\sqrt{2\beta}$) was assessed to 16.7 kJ·mol^{-1}. This value is higher than 8 kJ·mol^{-1}, suggesting that Pb(II) removal by the lignite was mainly chemical [17,46].

It is worth mentioning that compared to Langmuir model, the Freundlich one fits the experimental data better with lower APE and AIC values (Table 3).

This finding indicates that Pb(II) adsorption by the lignite happens heterogeneously on multilayer surfaces [47]. On the other hand, the Freundlich constant "n" exists in the range of 1–10 (5.1), indicating that Pb(II) adsorption by lignite is a favorable process. Similar value (5.13) was determined by Jellali *et al.* [19] when studying phosphorus removal efficiency by phosphate mine wastes. Moreover, the Langmuir's parameter "$R_L = (1/(1 + K_{L*C_0}))$" was estimated to 0.062 and 0.029 for initial Pb(II) concentrations of 80 and 175 mg·L^{-1}. These values were lower than 1 which confirms that lignite can be considered as a favorable media for Pb(II) adsorption.

The Langmuir's maximum adsorption capacity of Pb(II) by the lignite was assessed to 61.4 mg·g^{-1}for an initial aqueous pH of 5. It is about 2.0 and 7.2 higher than the values determined for raw lignites from Mongolia [15] and Turkey [48]. This adsorption capacity is also higher than the ones reported for other natural materials (Table 4) such as peanut shells [49] and rice husk [50]. This relatively high adsorption capacity of lignite witnesses the existence of important reactions between Pb(II) molecules and the lignite active sites. However, it is worth mentioning that this Pb(II) adsorption capacity remains lower than those reported for some activated carbons and biochars derived from agricultural wastes such as cypress sawdust [8] and peanut shell [49].

3.3. *Dynamic adsorption results*

The conservative tracer breakthrough curve (BTCs) for the three lignite bed heights were almost symmetric without the presence of any tailing when C/C_0 became close to 1 (data not shown). This finding demonstrates that under the used experimental conditions, the immobile water fraction inside the column is negligible [8]. During these tracer assays, the measured relative concentrations at the exit of the column become equal to 1 after durations of only 1.5 to 2 min for all the tested bed depths. This behavior confirms that there were no significant interactions between the Cl^- ions and the lignite particles.

The BTCs of Pb(II) through the different lignite bed heights appear much later compared to the tracer indicating that the Pb(II) is well adsorbed by lignite. Higher the lignite bed height (or mass), later the BTC appearance and also the adsorption sites saturation reaching ($C/C_0 = 1$) (Figure 8). For instance,

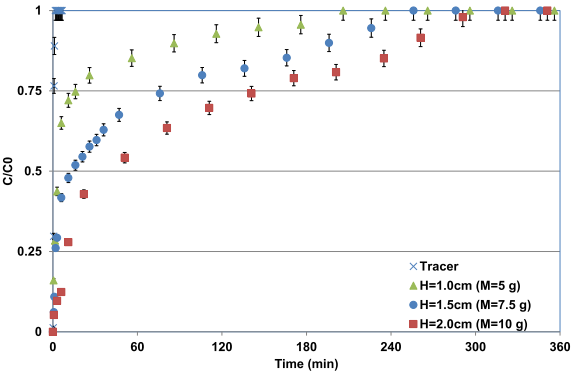

Figure 8. Observed Pb(II) breakthrough curves for different lignite bed heights ($C_0 = 100$ mg·L^{-1}; $pH_0 = 5$; $T = 20 \pm 2$ °C).

the plateau of $C/C_0 = 1$ was observed after durations of 206, 256, and 321 min corresponding to considerable synthetic solution volumes collected at the outlet of the column of about 12.4, 14.6, and 18.3 L for lignite bed depth heights of 1, 1.5, and 2 cm, respectively. This outcome is attributed to the fact that higher adsorbent bed heights contain more sorption sites permitting more adsorption of Pb(II) ions. Furthermore, the contact times between the pollutant and the lignite particles increase with the rising of the bed lignite height or mass. It has approximately doubled when the bed height increased from 1 to 2 cm. The Pb(II) adsorbed masses per gram of lignite, calculated according to (6), were 28.3, 41.2, and 48.7 mg·g^{-1} for bed heights of 1.0, 1.5, and 2.0 cm, respectively. The relatively low adsorbed amount for a bed height of 1 cm is mainly due to the very short contact time between Pb(II) and lignite particles. Similar trends were observed by Jellali *et al.* [8] and Jain *et al.* [53] when investigating metal removal by a biochar derived from the pyrolysis of $MgCl_2$-modifed cypress sawdust and a sunflower stem carbon–calcium alginate beads, respectively.

However, it is important to mention that the highest adsorption capacity obtained in column mode (48.7 mg·g^{-1}) was about 79% of the one obtained in batch mode (Section 3.1). This difference could be related to the short contact time in dynamic mode (lower than 1 min) compared to the batch mode (90 min). In column experiments, Pb(II) ions did not have sufficient time to exchange with the lignite

Table 4. Comparison of the used lignite removal efficiency of Pb(II) with lignites and other materials

Material	Assay type	Adsorption conditions	Pb(II) adsorption capacity ($mg \cdot g^{-1}$)	Reference
Raw lignite, Mongolia	Batch	C_0 = 200 $mg \cdot L^{-1}$; pH = −; D = 2.4 $g \cdot L^{-1}$; t = 3 h; T = room temperature	14.5	[15]
HNO_3 (10 $mol \cdot L^{-1}$) modified lignite, Mongolia			30.7	
Lignite washing plant tailings, Turkey		C_0 = 300 $mg \cdot L^{-1}$; pH = 9; D = 10 $g \cdot L^{-1}$; t = 2 h; T = room temperature	29.9	[48]
Raw lignite, Mikulčice, Czech Republic		C_0 = 10–500 $mg \cdot L^{-1}$; pH = 5.5; D = 5 $g \cdot L^{-1}$; t = 24 h; T = 25 °C	39.03*	[38]
Commercial lignite, India		C_0 = 10–50 $mg \cdot L^{-1}$; pH = 6; D = 10 $g \cdot L^{-1}$; t = 24 h; T = 30 °C	32.3	[51]
Peanut shell, Turkey		C_0 = 100–350 $mg \cdot L^{-1}$; pH = 5.5; D = 2 $g \cdot L^{-1}$; t = 3 h; T = 20 °C	32.9	[49]
Biomatrix from rice husk, India		C_0 = 50–200 $mg \cdot L^{-1}$; pH = 6; D = 3 $g \cdot L^{-1}$; t = 3 h; T = 32 °C	58.0	[50]
Biochar from treated cypress sawdust, Tunisia		C_0 = 200–600 $mg \cdot L^{-1}$; pH = 4; D = 2 $g \cdot L^{-1}$; t = 3 h; T = 20 °C	202.2	[8]
Commercial lignite, India	Column	C_0 = 50 $mg \cdot L^{-1}$; pH = 6.5; M = 0.5 g; Q = 1 $mL \cdot min^{-1}$; T = 30 °C	35.0	[51]
Raw cypress sawdust, Tunisia		C_0 = 100 $mg \cdot L^{-1}$; pH = 4; M = 10 g; Q = 59 $mL \cdot min^{-1}$; T = 20 °C	7.9	[8]
Biochar form cypress sawdust, Tunisia			97.1	
Chemically carbonized rubber wood sawdust, India		C_0 = 20 $mg \cdot L^{-1}$; pH = 5.2; M = 3.5 g; Q = 15 $mL \cdot min^{-1}$; T = 30 °C	37.0	[52]
Lignite, Cap Bon, Tunisia	Batch	C_0 = 80–175 $mg \cdot L^{-1}$; pH = 5; D = 2 $g \cdot L^{-1}$; t = 90 min; T = 20 °C	61.4	Current study
	Column	C_0 = 100 $mg \cdot L^{-1}$; pH = 5; H = 2 cm; Q = 60 $mL \cdot min^{-1}$; T = 20 °C	48.7	

*: mixture with Cu(II), Zn(II) and Cd(II).

particles. A similar finding was reported by Hannachi and Hafidh [54]. The authors demonstrated that the Pb(II) adsorption capacity by a bifunctionalized Xerogel in column mode was about 20% lower than the observed one in batch conditions. The obtained Pb(II) adsorbed amounts in column mode are higher than those of various natural materials including lignite [15,48] and other lignocellulosic materials [49, 50] even under static conditions. This outcome confirms that the lignite can be considered as an attractive and eco-friendly porous media for the removal of Pb(II) and other heavy metals and organics [55,56] from aqueous effluents.

3.4. *Raw and Pb(II)-loaded lignite characterization and adsorption mechanism exploration*

For a better assessment of the involved adsorption mechanisms during the removal of lead ions by lignite particles, as indicated in Section 2.1, multiple analysis techniques were used for the characterization of lignite before and after Pb(II) adsorption. The

examination of raw lignite samples by SEM analysis highlighted the heterogeneous aspect of this material bulk with surface presenting significant small scale height amplitude variation and low appearing porosity (Figure 9(a)). Furthermore, the images revealed a significant presence of the calcium carbonate and quartz suggesting their incorporation in the organic structure of lignite. A similar finding was reported by Oikonomopoulos *et al.* [57] for a Greek lignite. This is further confirmed by the EDX spectroscopy analysis where peaks related to calcium, silica, and other alkaline and alkaline earth metals were clearly identified (Figure 9(c)).

After lead adsorption, a dense layer of a most probably deposited Pb(II)on lignite surface (white contrast in the image (Figure 9(b)) can be seen. Moreover, EDX postadsorption spectroscopy showed the appearance of Pb(II) peaks which confirms its adsorption on the surface of lignite and its incorporation in the organic matrix (Figure 9(d)). It is worth highlighting that after the Pb(II) adsorption, all the EDX-detected peak intensities have significantly decreased which could be attributed to the involvement of these minerals and macroelements in the adsorption process. For instance, peak intensities related to C, O, and Fe have significantly decreased and those of calcium, magnesium, and potassium have almost disappeared after adsorption. These ascertainments suggest that the Pb(II) adsorption might be codriven by: (i) complexation with oxygenic functional groups, and by (ii) cation exchange, respectively.

Proximate analysis is a very interesting method to determine the variation in terms of macroelements present in the lignite feedstock before and Pb(II) adsorption [58]. Results depicted in the Figure 10 suggest that raw lignite is mainly composed of ash, volatile matter, and fixed carbonate percentages of 39.3%, 32.5%, and 21.2%, respectively.

These results are in agreement with the findings reported by Karatepe *et al.* [59] and Demirbas [60] when investigating macroelement content in various types of Turkish lignites using thermogravimetric analysis. After lead adsorption, a slight decrease was noticed in moisture, fixed carbon, and volatile matter contents by about 2.0%, 4.5%, and 2.1%, respectively. This observation could be related to the adsorption process of lead onto lignite aromatic structure where an exothermic process could be involved, leading to the release of water molecules and a slight fraction of organic carbon present in volatile matter [61]. On the other hand, ash content of the raw lignite has increased from 39.3% to more than 47.9% after Pb(II) retention (Figure 10). Despite the possible release minerals during adsorption process according to EDX analysis, the increase in ash content could be considered as an indicator of an increase in the mineral balance due to the retention of lead. According to Chouchene *et al.* [62], heavy metals existing as oxide forms are unlikely to be volatilized and remained present in the composition of ashes.

The mineral characterization of the raw lignite was determined through XRD analysis and its diffractograms are reported in Figure 11.

It is clear from the latter that lignite is characterized with a typical two-dimensional (002) peak at 25.03°. This reflection corresponds to the spacing between aromatic layers present in this raw material [63]. Moreover, two small bands were also noticed at 41.52° and 54.85° related to (10) and (11) spacing, suggesting a certain rearrangement of carbon into a graphite-like structure. These three peaks remained distinguishable after lead adsorption (Figure 11). Figure 11 also shows that lignite is characterized with a relatively high presence of quartz (SiO_2). Moreover, polymorphous mineral structure of silica are in the form of cristobalite and mullite, indicating the presence of heavy metals, alkali, and alkaline earth metals such as Fe, Al, K, Na, Mn, Mg, and P [64]. After Pb(II) adsorption, three distinguishable peaks appeared at 27.7°, 43.7° and 44.5°, respectively, corresponding to a crystalline form of lead sulfate ($PbSO_4$) (Figure 11). The decrease in intensity or even the disappearance of certain peaks was noticed for the case of calcium carbonate ($CaCO_3$) and phosphorus nitrogen chloride ($(PNCl_2)_4$). This finding is in concordance with the isotherm results suggesting a possible chemical adsorption process mainly driven by an ion-exchange reaction.

The FTIR analysis has been used to identify the main surface active functional groups on the lignite surface and especially those involved in the Pb(II) adsorption. FTIR spectra of lignite before and after Pb(II) removal are presented in Figure 12. Initially, the heterogeneous aspect of lignite surface was confirmed by the presence of both acid and basic functional groups at different intensities. The peak at 3392 cm^{-1} corresponds to O–H group stretch and is directly related to possible lignocellulosic-derived

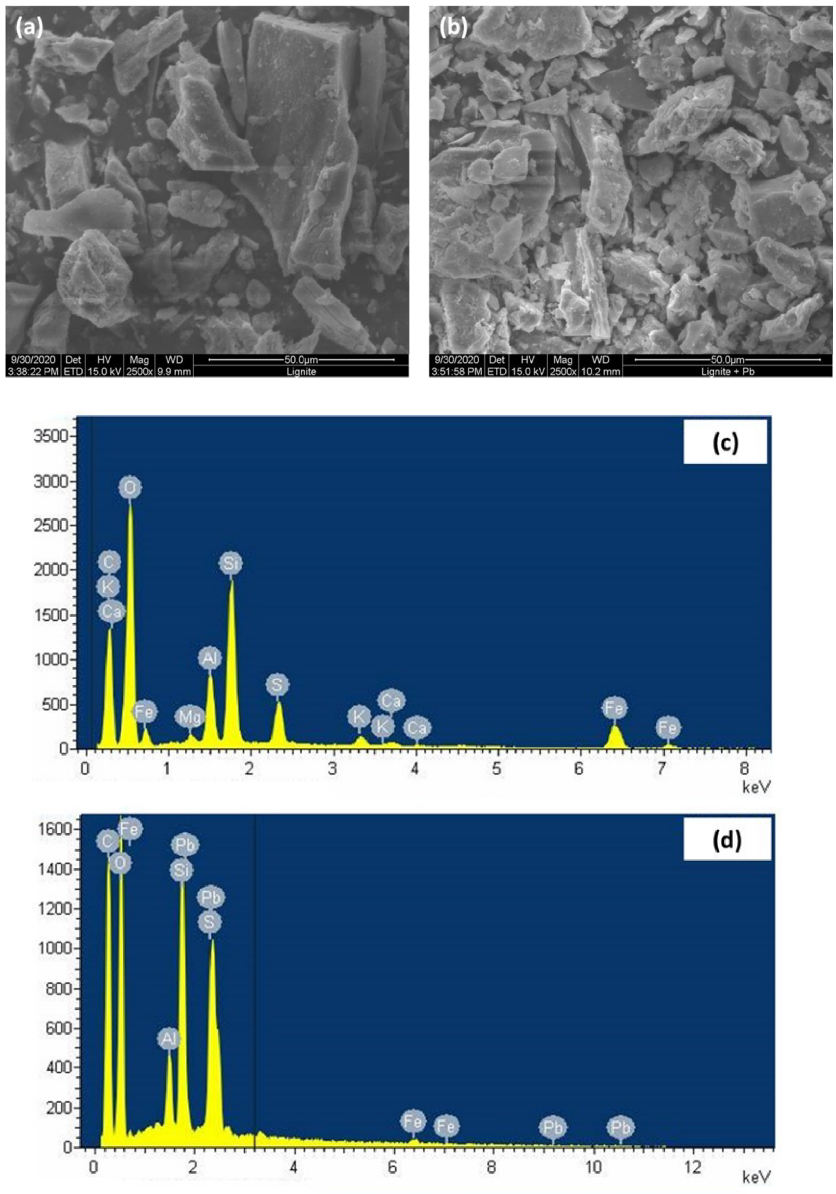

Figure 9. SEM images of (a) raw and (b) Pb(II)-loaded lignite and (c,d) their respective EDX spectra.

content in lignite. It is connected to alcohol, carboxyl, and hydroxyl groups from cellulose or phenols from lignin [65]. Peaks detected at 2920 cm^{-1} and 2850 cm^{-1} are related to C–H aliphatic stretches. The bands at 1691 cm^{-1} was assigned to a C=O bond stretching in aldehydes or carboxylic acids. The stretch recorded at 1610 cm^{-1} corresponds to the C=C aromatic skeletal. Moreover, stretching in bands recorded at 1097 cm^{-1} and 910 cm^{-1} are related to C–O, while peaks found between 794 cm^{-1} and 601 cm^{-1} are attributed to C–H bend in aromatic groups.

After Pb (II) adsorption, the FTIR spectrum presented an almost similar aspect to the original feedstock with few marked modifications. In fact, a shift in O–H group by +25 cm^{-1} was recorded. Moreover,

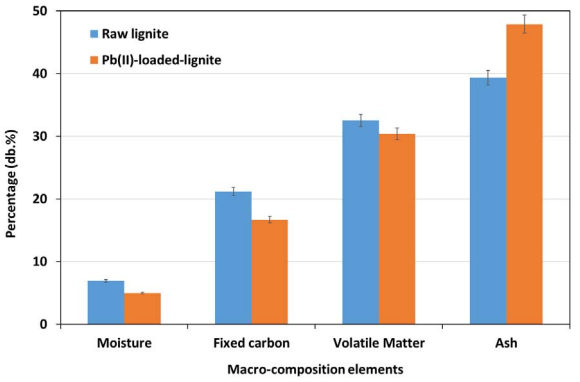

Figure 10. Proximate analysis of raw and Pb(II)-loaded lignite.

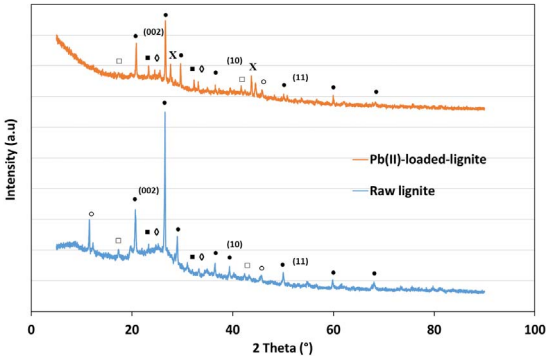

Figure 11. XRD diagrams for raw and Pb(II)-loaded lignite (•: SiO_2, □: $CaCO_3$; ◇: mullite; ■: cristobalite; ○: $(PNCl_2)_4$; **X**: $PbSO_4$).

a shift by about −13 cm^{-1} was noted for –C–H groups between 1610 cm^{-1} and 1590 cm^{-1} (Figure 12). Similar behavior was found for –C–H groups between 800 cm^{-1} and 600 cm^{-1}, which displayed a slight shift of +4 cm^{-1}. Similarly, peaks related to aliphatic functional groups decreased in intensity after Pb(II) adsorption with a recorded shift of −4 cm^{-1}. A singularity was detected for the peak assigned to C=C, which gained in intensity and shifted from 1371 cm^{-1} to 1382 cm^{-1} after adsorption. According to Shrestha *et al.* [61], the changes in intensities and the location shifts observed for characterizing FTIR peaks cannot be attributed to an electrostatic interaction between metallic ions and the surface. It is interpreted as a possible complexation reaction between lead ions and the functional groups. Accordingly, lead removal was favored by a possible complexation reaction with

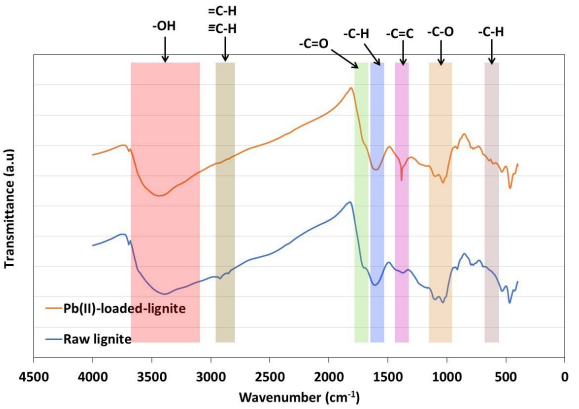

Figure 12. FTIR analyses of lignite before and after Pb(II) adsorption.

hydroxyl, aliphatic, carboxylic, and aromatic functional groups [66]. This reaction is mainly driven by an ion-exchange mechanism through the release of cations from lignite surface and the retention of Pb^{2+} ions instead. Similar findings were reported by Pehlivan and Arslan [41] when studying the removal of three bivalent metals, namely Cu^{2+}, Pb^{2+}, and Ni^{2+} using lignite and coconut shell-based activated carbon fiber.

4. Conclusions

This research work proves that lignite can be considered as a promising and attractive material for Pb(II) removal from aqueous effluents under wide static and dynamic experimental conditions. This attractiveness is supported by the exceptional rapid (only few minutes) and high (61.4 and 48.7 $mg{\cdot}g^{-1}$ for batch and columns tests) adsorption capacity compared to other lignites and lignocellulosic-derived adsorbents. The batch kinetic and isothermal modeling studies as well as the specific analyses on the structure and texture of lignite before and after Pb(II) removal, showed that this adsorption process is mainly chemical and occurs heterogeneously on multilayer surfaces. Besides complexation with some specific functional groups (hydroxyl, carboxylic, and phenolic groups), this process might include cation exchange with some cations such as calcium, magnesium, potassium, and sodium. Further investigations will be undertaken in order to: (i) assess the Pb(II)

desorption and lignite regeneration in batch and dynamic mode, (ii) the adsorption/desorption by lignite of other heavy metals in single and mixed modes.

Acknowledgments

The authors gratefully acknowledge the Tunisian Ministry of Higher Education and Scientific Research for financing this research project.

References

[1] C. V. Mohod, J. Dhote, *Int. J. Innov. Res. Sci. Eng. Technol.*, 2013, **2**, 2992-2996.
[2] S. Tong, Y. E. Von Schirnding, T. Prapamontol, *Bull. World Health Organ.*, 2000, **78**, 1068-1077.
[3] N. Bensacia, I. Fechete, S. Moulay, O. Hulea, A. Boos, F. Garin, *C. R. Chim.*, 2014, **17**, 869-880.
[4] S. Jellali, M. Labaki, A. A. Azzaz, H. Akrout, L. Limousy, M. Jeguirim, "7 - Biomass-derived chars used as adsorbents for liquid and gaseous effluents treatment", in *Char and Carbon Materials Derived from Biomass*, Elsevier, 2019, 229-290.
[5] A. A. Azzaz, S. Jellali, H. Akrout, A. A. Assadi, L. Bousselmi, *J. Clean. Prod.*, 2018, **201**, 28-38.
[6] K. Haddad, M. Jeguirim, B. Jerbi, A. Chouchene, P. Dutournié, N. Thevenin, L. Ruidavets, S. Jellali, L. Limousy, *ACS Sustain. Chem. Eng.*, 2017, **5**, 8988-8996.
[7] L. Joseph, B. M. Jun, J. R. V. Flora, C. M. Park, Y. Yoon, *Chemosphere*, 2019, **229**, 142-159.
[8] S. Jellali, E. Diamantopoulos, K. Haddad, M. Anane, W. Durner, A. Mlayah, *J. Environ. Manage.*, 2016, **180**, 439-449.
[9] B. O. Otunola, O. O. Ololade, *Environ. Technol. Innov.*, 2020, **18**, article no. 100692.
[10] K. Haddad, S. Jellali, S. Jaouadi, M. Benltifa, A. Mlayah, A. H. Hamzaoui, *C. R. Chim.*, 2015, **18**, 75-87.
[11] I.E. Agency, "Coal Information: Overview", 2020.
[12] T. Arjumend, M. K. Abbasi, E. Rafique, *Pakistan J. Bot.*, 2015, **47**, 2231-2238.
[13] A. Gürses, A. Hassani, M. Kranşan, Ö. Açşl, S. Karaca, *J. Water Process Eng.*, 2014, **2**, 10-21.
[14] A. Rostvall, W. Zhang, W. Dürig, G. Renman, K. Wiberg, L. Ahrens, P. Gago-ferrero, *Water Res.*, 2018, **137**, 97-106.
[15] B. Huang, G. Liu, P. Wang, X. Zhao, H. Xu, *Processes*, 2019, **7**, article no. 167.
[16] A. A. Azzaz, S. Jellali, R. Souissi, K. Ergaieg, L. Bousselmi, *Environ. Sci. Pollut. Res.*, 2017, **24**, 18240-18256.
[17] A. A. Azzaz, S. Jellali, A. A. Assadi, L. Bousselmi, *Desalin. Water Treat.*, 2016, **57**, 22107-22119.
[18] A. Ibn Ferjani, M. Jeguirim, S. Jellali, L. Limousy, C. Courson, H. Akrout, N. Thevenin, L. Ruidavets, A. Muller, S. Bennici, *Renew. Sustain. Energy Rev.*, 2019, **107**, 425-443.
[19] S. Jellali, M. A. Wahab, R. B. Hassine, A. H. Hamzaoui, L. Bousselmi, *Chem. Eng. J.*, 2011, **169**, 157-165.
[20] K. Mahmoudi, N. Hamdi, M. Ben Ali, S. Jellali, E. Srasra, *C. R. Chim.*, 2020, **23**, 689-704.
[21] S. Hadroug, S. Jellali, J. J. Leahy, M. Kwapinska, M. Jeguirim, H. Hamdi, W. Kwapinski, *Water*, 2019, **11**, article no. 2271.
[22] K. Haddad, S. Jellali, M. Jeguirim, A. Ben Hassen Trabelsi, L. Limousy, *J. Environ. Manage.*, 2018, **216**, 305-314.
[23] M. M. Dávila-Jiménez, M. P. Elizalde-González, E. García-Díaz, M. González-Perea, M. R. G. Guevara-Villa, *Adsorp. Sci. Technol.*, 2014, **32**, 605-522.
[24] S. Jellali, E. Diamantopoulos, H. Kallali, S. Bennaceur, M. Anane, N. Jedidi, *J. Environ. Manage.*, 2010, **91**, 897-905.
[25] S. Milicevic, T. Boljanac, S. Martinovic, M. Vlahovic, V. Milosevic, B. Babic, *Fuel Process. Technol.*, 2012, **95**, 1-7.
[26] D. Pentari, V. Perdikatsis, D. Katsimicha, A. Kanaki, *J. Hazard. Mater.*, 2009, **168**, 1017-1021.
[27] U. Rozman, G. Kalčíková, G. Marolt, T. Skalar, A. Žgajnar Gotvajn, *Environ. Technol. Innov.*, 2020, **18**, article no. 100742.
[28] M. Banerjee, R. K. Basu, S. K. Das, *Environ. Sci. Pollut. Res.*, 2019, **26**, 11542-11557.
[29] D. Mohan, S. Chander, *J. Colloid Interface Sci.*, 2006, **299**, 76-87.
[30] C. Gunawardana, P. Egodawatta, A. Goonetilleke, *Environ. Pollut.*, 2014, **184**, 44-53.
[31] T. Okuda, *Atmos. Environ.*, 2013, **75**, 1-5.
[32] P. N. Ikenyiri, C. P. Ukpaka, *J. Chem. Eng. Process Technol.*, 2016, **7**, 5-8.
[33] P. Suresh Kumar, L. Korving, K. J. Keesman, M. C. M. van Loosdrecht, G. J. Witkamp, *Chem. Eng. J.*, 2019, **358**, 160-169.
[34] L. Dong, S. Pan, Z. Wang, *Water Air Soil Pollut.*, 2020, **231**, article no. 230.
[35] S. Jellali, M. A. Wahab, M. Anane, K. Riahi, N. Jedidi, *Desalination*, 2011, **270**, 40-49.
[36] H. Akrout, S. Jellali, L. Bousselmi, *C. R. Chim.*, 2015, **18**, 110-120.
[37] M. Jain, V. K. Garg, U. K. Garg, K. Kadirvelu, M. Sillanpää, *Int. J. Environ. Res.*, 2015, **9**, 1079-1088.
[38] L. Doskočil, M. Pekař, *Fuel Process. Technol.*, 2012, **101**, 29-34.
[39] I. Tsibranska, E. Hristova, *Bulg. Chem. Commun.*, 2011, **43**, 370-377.
[40] M. Jain, M. Yadav, T. Kohout, M. Lahtinen, V. K. Garg, M. Sillanpää, *Water Resour. Ind.*, 2018, **20**, 54-74.
[41] E. Pehlivan, G. Arslan, *Fuel Process. Technol.*, 2007, **88**, 99-106.
[42] A. Mlayah, S. Jellali, *Int. J. Environ. Sci. Technol.*, 2015, **12**, 2965-2978.
[43] M. Jain, V. K. Garg, K. Kadirvelu, *Desalin. Water Treat.*, 2014, **52**, 5681-5695.
[44] M. Jain, M. Yadav, S. Chaudhry, *Toxin Rev.*, 2020, 1-14.
[45] M. A. Binabaj, S. M. N. N. Ramezanian, *Int. J. Environ. Sci. Technol.*, 2018, **15**, 1509-1520.
[46] S. Valliammai, Y. Subbareddy, K. S. Nagaraja, B. Jeyaraj, *Indian J. Chem. Technol.*, 2017, **24**, 134-144.
[47] S. Gao, D. Wang, S. R. Dangi, Y. Duan, T. Pflaum, J. Gartung, R. Qin, T. Turini, *Sci. Total Environ.*, 2020, **714**, article no. 136432.
[48] M. Uçurum, *Fuel*, 2009, **88**, 1460-1465.
[49] Ş. Taşar, F. Kaya, A. Özer, *J. Environ. Chem. Eng.*, 2014, **2**, 1018-1026.
[50] K. K. Krishnani, X. Meng, C. Christodoulatos, V. M. Boddu, *J. Hazard. Mater.*, 2008, **153**, 1222-1234.
[51] R. Rao, M. Khan, F. Rehman, *Adsorp. Sci. Technol.*, 2011, **29**, 83-98.

[52] S. Biswas, U. Mishra, *J. Chem.*, 2015, **2015**, article no. 495257.
[53] M. Jain, V. K. Garg, K. Kadirvelu, M. Sillanpää, *Ind. Eng. Chem. Res.*, 2015, **54**, 1419-1425.
[54] Y. Hannachi, A. Hafidh, *J. Saudi Chem. Soc.*, 2020, **24**, 505-519.
[55] C. Chokejaroenrat, A. Watcharenwong, *Water Air Soil Pollut.*, 2020, **231**, article no. 249.
[56] A. Hassani, F. Vafaei, S. Karaca, A. R. Khataee, *J. Ind. Eng. Chem.*, 2014, **20**, 2615-2624.
[57] I. K. Oikonomopoulos, M. Perraki, N. Tougiannidis, T. Perraki, M. J. Frey, P. Antoniadis, W. Ricken, *Int. J. Coal Geol.*, 2013, **115**, 1-12.
[58] A. A. Azzaz, M. Jeguirim, V. Kinigopoulou, C. Doulgeris, M. L. Goddard, S. Jellali, C. Matei Ghimbeu, *Sci. Total Environ.*, 2020, **733**, article no. 139314.
[59] N. Karatepe, S. Küçükbayrak, *Thermochim. Acta*, 1993, **213**, 147-150.
[60] A. Demirbas, *Util. Environ. Eff.*, 2008, **30**, 1876-1883.
[61] S. Shrestha, G. Son, S. H. Lee, T. G. Lee, *Chemosphere*, 2013, **92**, 1053-1061.
[62] A. Chouchene, M. Jeguirim, G. Trouvé, *Clean Technol. Environ. Policy*, 2014, **16**, 979-986.
[63] J. Wang, Y. He, H. Li, J. Yu, W. Xie, H. Wei, *Fuel*, 2017, **203**, 764-773.
[64] R. K. Vempati, A. Rao, T. R. Hess, D. L. Cocke, H. V. Lauer, *Cem. Concr. Res.*, 1994, **24**, 1153-1164.
[65] S. Guo, X. Dong, T. Wu, F. Shi, C. Zhu, *J. Anal. Appl. Pyrol.*, 2015, **116**, 1-9.
[66] L. Dong, L. Hou, Z. Wang, P. Gu, G. Chen, R. Jiang, *J. Hazard. Mater.*, 2018, **359**, 76-84.